HHS Public Access

Author manuscript

Radiat Res. Author manuscript; available in PMC 2018 March 01.

Published in final edited form as:

Radiat Res. 2017 March ; 187(3): 367–381. doi:10.1667/RR14623.1.

MnTE-2-PyP Treatment, or NOX4 Inhibition, Protects against Radiation-Induced Damage in Mouse Primary Prostate Fibroblasts by Inhibiting the TGF-Beta 1 Signaling Pathway

Arpita Chatterjee, **Elizabeth A. Kosmacek**, and **Rebecca E. Oberley-Deegan**[1]

Department of Biochemistry and Molecular Biology, University of Nebraska Medical Center, Omaha, Nebraska 68198

Abstract

Prostate cancer patients who undergo radiotherapy frequently suffer from side effects caused by radiation-induced damage to normal tissues adjacent to the tumor. Exposure of these normal cells during radiation treatment can result in tissue fibrosis and cellular senescence, which ultimately leads to postirradiation-related chronic complications including urinary urgency and frequency, erectile dysfunction, urethral stricture and incontinence. Radiation-induced reactive oxygen species (ROS) have been reported as the most potent causative factor for radiation damage to normal tissue. While MnTE-2-PyP, a ROS scavenger, protects normal cells from radiation-induced damage, it does not protect cancer cells during radiation treatment. However, the mechanism by which MnTE-2-PyP provides protection from radiation-induced fibrosis has been unclear. Our current study reveals the underlying molecular mechanism of radiation protection by MnTE-2-PyP in normal mouse prostate fibroblast cells. To investigate the role of MnTE-2-PyP in normal tissue protection after irradiation, primary prostate fibroblasts from C57BL/6 mice were cultured in the presence or absence of MnTE-2-PyP and exposed to 2 Gy of X rays. We found that MnTE-2-PyP could protect primary prostate fibroblasts from radiation-induced activation, as measured by the contraction of collagen discs, and senescence, detected by beta-galactosidase staining. We observed that MnTE-2-PyP inhibited the TGF-β-mediated fibroblast activation pathway by downregulating the expression of TGF-β receptor 2, which in turn reduced the activation and/or expression of SMAD2, SMAD3 and SMAD4. As a result, SMAD2/3-mediated transcription of profibrotic markers was reduced by MnTE-2-PyP. Due to the inhibition of the TGF-β pathway, fibroblasts treated with MnTE-2-PyP could resist radiation-induced activation and senescence. NADPH oxidase 4 (NOX4) expression is upregulated after irradiation and produces ROS. As was observed with MnTE-2-PyP treatment, $NOX4^{-/-}$ fibroblasts were protected from radiation-induced fibroblast activation and senescence. However, $NOX4^{-/-}$ fibroblasts had reduced levels of active TGF-β1, which resulted in decreased TGF-β signaling. Therefore, our data suggest that reduction of ROS levels, either by MnTE-2-PyP treatment or by eliminating NOX4 activity, significantly protects normal prostate tissues from radiation-induced tissue damage, but that these approaches work on different components of the TGF-β signaling pathway. This study proposes a crucial insight into the molecular mechanism executed by MnTE-2-PyP when utilized as a

[1]Address for correspondence: Department of Biochemistry and Molecular Biology, Room 7014 DRC1, 985870 Nebraska Medical Center, Omaha, NE 68106; becky.deegan@unmc.edu.

radioprotector. An understanding of how this molecule works as a radioprotector will lead to a better controlled mode of treatment for post therapy complications in prostate cancer patients.

Introduction

Radiation therapy is a common treatment for prostate cancer, which is the second major cause of cancer related mortality among men (1). Although there are sophisticated measures for precise delivery of radiotherapy to the tumor tissue, radiation-induced damage nevertheless occurs in the normal healthy tissue surrounding the tumor. The side effects of radiation therapy observed in prostate cancer patients include bowel and rectal wall damage, urinary urgency and frequency, erectile dysfunction and urethral stricture (2, 3). In addition, as a response to radiation-induced bystander effect, irradiated nontumor cells can cause radiation resistance and recurrence to the tumor cell (4, 5). Radiation treatment induces the production of reactive oxygen species (ROS), which are thought to be responsible for radiation-induced normal tissue injury. Irradiated fibroblast cells of normal tissue can be activated to become myofibroblasts, which ultimately cause tissue fibrosis, or they may become senescent, which also affects the normal physiology of the tissue (6–8). These events result in the onset of tissue damage and radiation-induced chronic side effects, ultimately affecting the quality of life for these patients. Therefore, a potent normal tissue protector is needed for patients undergoing radiation therapy for prostate cancer.

A successful radioprotector should protect normal tissue, but not the tumor, from radiation-induced damage. Manganese (III) Meso-Tetrakis-(N-Ethylpyridinium-2-yl) (MnTE-2-PyP, T2E), is a molecule that can scavenge ROS, including superoxide, lipid peroxides and peroxynitrite. Previously reported studies have shown that MnTE-2-PyP can protect from radiation-induced external tissue damage in rats (9), without protecting the tumor (10). MnTnBuOE-2-PyP, a sister compound of MnTE-2-PyP, has been shown to protect normal colorectal fibroblast cells, while simultaneously enhancing the cytotoxic effects of radiation or chemotherapeutic agents on colorectal cancer cells (11). Understanding the mechanism by which a compound works is helpful for successful clinical use. Since the majority of prostate cancers are treated with radiotherapy, the purpose of this study was to investigate whether MnTE-2-PyP can protect normal prostate fibroblast cells from radiation-induced damage, and to investigate the molecular mechanism of MnTE-2-PyP activity in irradiated prostate fibroblast cells.

TGF-β1 and NOX4 are reported as two central regulatory molecules involved in radiation-induced fibrosis, inflammation and senescence. Among the five NOX isoforms, NOX4 is primarily reported to be responsible for the TGF-β-induced profibrotic response (12–18). NOX4 activity is increased after irradiation and is thought to be one of the main sources of ROS after irradiation. TGF-β can increase the expression of NOX4 (15). On the other hand, siRNA-mediated knockdown of NOX4 results in downregulation of TGF-β1 target genes (13). Therefore, there is a reciprocal relationship between these two central regulatory molecules of fibrotic disease (15), and so it was also necessary to study whether MnTE-2-PyP can affect the TGF-β signaling pathway.

To address these goals, we used primary mouse prostate fibroblasts as an in vitro model of radiation-induced fibroblast activation. In the current study, we observed that after 2 Gy X-ray irradiation, MnTE-2-PyP significantly reduced radiation-induced activation and senescence of primary mouse prostate fibroblasts. TGF-β1-mediated fibro-blast activation and NOX4-TGF-β1-mediated cellular senescence are well-studied pathways in fibrotic disease (19–21). Therefore, previous pharmacological attempts to deal with radiation-induced fibrosis and senescence have focused on inhibition of TGF-β1 (22, 23). Taking this into consideration, we have measured MnTE-2-PyP regulation of the TGF-β1 signaling pathway as one mechanism of its action as a radioprotector. Although MnTE-2-PyP does not significantly reduce the extracellular TGF-β1 levels, MnTE-2-PyP inhibits TGF-β receptor 2 expression, which results in the suppression of TGF-β1 target gene expression. Since TGF-β1 is one of the central regulators of the fibrotic response after irradiation, it is necessary to investigate whether MnTE-2-PyP can block the effect of TGF-β1-mediated signaling after irradiation to the same extent as a specific pharmacological inhibitor of TGF-β1 signaling. We found that MnTE-2-PyP inhibits fibroblast activation as well as the TGF-β1 inhibitor, SB431542, in the presence and absence of radiation. We also investigated the role of NOX4 in radiation-induced fibrosis. We found that NOX4$^{-/-}$ primary prostate fibroblasts were protected from radiation-induced activation and senescence by reducing extracellular TGF-β1 levels as well as reducing the expression of Smad3 and phosphorylation of Smad2, which are downstream targets of TGF-β1. These data suggest that reducing ROS with MnTE-2-PyP treatment, or NOX4 inhibition, results in the protection of normal tissues by inhibition of the TGF-β1 signaling pathway.

Materials and Methods

Animals

Wild-type and NOX4$^{-/-}$ male C57BL/6 mice (Jackson Laboratory, Bar Harbor, ME), 8–10 weeks of age, were housed at the University of Nebraska Medical Center (UNMC; Omaha, NE) and kept on a 12:12 h light-dark schedule with *ad libitum* food and water. All mice were treated according to the Care and Use of Laboratory Animals Guide of National Institutes of Health, and animal protocol was approved by the Institutional Animal Care and Use Committee at UNMC.

Primary Prostate Fibroblast Isolation and Culture Conditions

The prostates were collected from 8-to-10-week-old wild-type and NOX4$^{-/-}$ C57BL/6 mice. Prostates were then minced, and digested by 5 mg/ml Gibco® Collagenase Type I (cat. no. 17100017; Thermo Fisher Scientific Inc., Rockford, IL) for 30 min at 37°C (24). Tissue fragments were then cultured for 2–3 weeks in Dulbecco's minimal essential media (DMEM) supplemented with 10% fetal bovine serum (FBS), 1% penicillin/streptomycin and 1% nonessential amino acids with or without 30 μ*M* MnTE-2-PyP (a gift from Dr. James Crapo, National Jewish Health, Denver, CO; for wild-type cells only). After five days of culture, all the cells were fibroblasts. Purity of the cells was determined by ER-TR7 (cat. no. 73355; Santa Cruz Biotechnology® Inc., Dallas, TX), a fibroblast marker, and by Keratin 17 (cat. no. 4543; Cell Signaling Technology®, Danvers, MA), an epithelial cell marker. All

experiments were repeated in triplicate using primary fibroblast cells collected from prostates of different mice.

Measurement of Superoxide and Other ROS

To measure the superoxide and overall ROS production, 2-week-old primary prostate fibroblast cells were seeded at a concentration of 1×10^6 cells/flask in the presence or absence of 30 μ*M* MnTE-2-PyP or an equal volume of phosphate buffered saline (PBS). Cells were then either sham irradiated or 2 Gy X-ray irradiated (RS 2000; Rad Source Technologies Inc., Alpharetta, GA). At 24 h postirradiation, cells were harvested by trypsinization. After washing, cells were stained with 50 μ*M* of dihydroethidium (DHE) for 20 min at 37°C in the dark and then subjected to flow cytometric analysis using LSRII Green 532 Flow Cytometer (BD Biosciences, San Jose, CA). To measure superoxide specifically, 405/570 nm excitation/emission was used. To measure all ROS products, 488/540 nm excitation/emission wavelengths were used. Data were analyzed using FACSDiva™ analysis software (BD Biosciences).

Cell Size Estimation

Two-week-old primary prostate fibroblast cells were seeded at a concentration of 2×10^5 cells/flask in the presence or absence of 30 μ*M* MnTE-2-PyP or an equal volume of PBS. Cells were then either sham irradiated or 2 Gy X-ray irradiated. At 48 h postirradiation, the cells were imaged using a Leica inverted phase contract microscope. Images were analyzed using ImageJ software (NIH, Bethesda, MD). Approximately 1,000 cell borders were marked per treatment group. Cell areas were converted to μm^2 using a conversion factor of 11.8 pixels/μm. GraphPad Prism 6 software (GraphPad Software Inc., La Jolla, CA) was used to analyze the distributions of cell size in each group.

Collagen Contraction Assay

Cells (4×10^5/T25 flask) were seeded in the presence of 30 μ*M* MnTE-2-PyP or 1 μ*M* SB431542 (TGF-β1 inhibitor, cat. no. 4317; Sigma-Aldrich® LLC, St. Louis, MO), or an equal volume of PBS. The following day, the cells were either treated with 5 ng/ml of TGF-β1 (cat. no. 580702; BioLegend® Inc., San Diego, CA) in serum-free media or irradiated (sham or 2 Gy X rays). After 48 h of incubation at 37°C in 5% CO_2, cells were harvested and 1×10^5 cells per 500 μl were replated in 10× DMEM containing 0.5 *M* NaOH, 2 mg/ml rat tail collagen (cat. no. 354249; Corning® Inc., Corning, NY) and 10% FBS in low-attachment 24-well plates. After solidification of collagen, discs were released from the sides of the well, and suspended in 500 μl complete growth media incubated for 12 h for contraction of collagen discs. After incubation, discs were imaged and the area measured using ImageJ software (25).

Senescence Assay

Cells (2×10^5/T25 flask) were seeded in presence of 30 μ*M* MnTE-2-PyP or an equal volume of PBS. After 24 h, the cells were either sham irradiated or 2 Gy X-ray irradiated. At 48 h postirradiation, cells were fixed in 4% PFA in PBS for 3 min. After washing twice with PBS for 5 min, the cells were covered with SA-β-Gal staining solution (0.1% X-gal, 5 m*M*

potassium ferrocyanide, 5 m*M* potassium ferricyanide, 150 m*M* sodium chloride, and 2 m*M* magnesium chloride in 40 m*M* citric acid/sodium phosphate solution, pH 6.0) (26), followed by a further incubation at 37°C avoiding light exposure. After approximately 24 h of incubation, cells were imaged by a brightfield Olympus® IX81 inverted microscope (Olympus America Inc., Melville, NY). Images were analyzed with ImageJ after inverting to aid visibility of SA-β-gal-positive cells and enumerated for senescence (pink) staining (25).

Profibrotic Gene Expression PCR Array

Cells (1×10^6/T25 flask) were seeded in the presence of 30 μ*M* MnTE-2-PyP or an equal volume of PBS. The following day, cells were either sham irradiated or 2 Gy X-ray irradiated. At 24 h postirradiation, cells were harvested and washed two times with 1× PBS, and total cellular RNA was then isolated using Quick-RNA™ MiniPrep (Plus) kit (Zymo Research Corp., Irvine, CA) following the manufacturer's protocol. Concentration and quality of total RNA were measured with Infinite® M200 PRO plate reader (Tecan®, Männedorf, Switzerland). Total RNAs having a 260/280 ratio of ~2.0 were used for further experiments. Total RNA (3 μg) from each sample was subjected to cDNA preparation using iScript™ Reverse Transcription Supermix (cat. no. 170-8840; Bio-Rad Laboratories Inc., Hercules, CA). Total cDNA of each sample was diluted to the required volume using DNase/RNase free water. Then, cDNA was used to amplify the profibrotic genes predesigned in Fibrosis Tier 1 M96 PrimePCR array plates (Bio-Rad) by using SsoAdvanced™ Universal SYBR® Green Supermix (cat. no. 172-5271; Bio-Rad Laboratories). The same amount of cDNA was used to study the expression of RPLP0 genes as another internal control, using manually designed primers. All PCR analyses were performed in a Bio-Rad CFX96™ real-time thermal cycler. Primers for GAPDH used as the internal control gene were provided in the PrimePCR plate. PrimePCR data were analyzed using Bio-Rad CFX Manager software version 3.1. Log_2 expression data of irradiated samples treated with MnTE-2-PyP were plotted against the irradiated sample treated with PBS.

TGF-Beta 1 ELISA

Cells (2×10^6/T75 flask) were seeded in the presence of 30 μ*M* MnTE-2-PyP or an equal volume of PBS. The following day, the cells were either sham or 2 Gy X-ray irradiated. After 24 h postirradiation, conditioned media from each experimental condition were collected. A TGF-β1 standard or conditioned media were added to respective wells of the ELISA plate coated with TGF-β1 antibody. The protocol, provided in the mouse TGF-β1 ELISA kit (cat. no. DY1679-05; R&D Systems™, Minneapolis, MN), was performed according to the manufacturer's instructions.

Western Blot

Cells (2×10^6 cells/T75 flask) were seeded in the presence of 30 μ*M* MnTE-2-PyP or an equal volume of PBS for 24 h before either sham or 2 Gy irradiation and 24 h later the cells were collected and washed in 1× PBS. Cell pellets were lysed by cell lysis buffer [120 m*M* NaCl, 50 m*M* Tris-HCl, 5 m*M* EDTA, 1% NP-40 and complete protease inhibitor cocktail tablets (1 tablet/50 ml, cat. no. 11697498001; Roche Diagnostics, Indianapolis, IN)]. After incubation for 30 min on ice, cell lysates were sonicated for 8–10 pulses at 80% amplitude. After sonication, lysates were centrifuged at 4°C for 15 min at 11,000g and supernatants

were collected. Whole cell lysates were assayed for total protein concentrations with a Bradford reagent (Amresco® Inc., Solon, OH) using bovine serum albumin as a standard. Total proteins (40 μg) were loaded on to Bolt® 4–12% Bis-Tris Plus gels (Thermo Fisher Scientific) and transferred to nitrocellulose membranes (Life Technologies, Grand Island, NY). After incubation with 5% nonfat milk in TBST (10 m*M* Tris, pH 8.0, 150 m*M* NaCl, 0.5% Tween™ 20) for 2 h, the membranes were incubated with primary antibodies overnight. Membranes were then washed with TBST and incubated with a 1:10,000 dilution of HRP-conjugated secondary antibodies for 1 h at room temperature. Blots were then washed with TBST and developed with an ECL detection system (Thermo Fisher Scientific) and exposed to film. Films were scanned, and densitometry analyses of the scanned images were performed using ImageJ. Ponceau-stained total protein was used as the loading control for each blot. For this study, the following primary and secondary antibodies were used: TGF-β receptor 2 [1:1,000 dilution (cat. no. sc-400; Santa Cruz Biotechnology)]; phospho-Smad2 (Ser 465/ 467) (1:1,000 dilution, cat. no. 3101), Smad2 (1:1,000 dilution, cat. no. 5339), phospho-Smad3 (Ser 423/425) (1:500 dilution, cat no. 9520) and Smad3 (1:1,000 dilution, cat. no. 9523), all from Cell Signaling Technology; Smad4 (1:2000 dilution, cat. no. ab40759; Abcam); Smad7 (1:1,000 dilution, cat. no. sc-11392) and Pai-1 (1:500 dilution; cat. no. sc-8979), both from Santa Cruz Biotechnology; and anti-Rabbit secondary (1:10,000 dilution, cat. no. A24537; Life Technologies).

Statistical Analyses

GraphPad Prism 6 software version 6.0.5 for Windows was used for all the statistical analyses. Unless otherwise indicated, values are the mean and standard deviation from three independent experiments. A statistically significant difference was determined for cell size, collagen contraction and senescence by one-way analysis of variance (ANOVA) followed by post hoc Tukey's test for multiple comparisons. One-way ANOVA followed by Holm-Sidak correction for multiple comparisons was used to compare the differences among three groups in the case of external TGF-β1 measurement by ELISA and measurement of protein expression by Western blot.

Results

MnTE-2-PyP Reduces Radiation-Induced Superoxide and Other ROS Production

Exposure to radiation produces high levels of ROS, including superoxide. MnTE-2-PyP is a superoxide scavenger, but in certain cell types MnTE-2-PyP can also act as a pro-oxidant. To determine the role of MnTE-2-PyP in a normal fibroblast redox state, we measured DHE activation. Excitation at 405 nm can specifically measure superoxide, whereas 488 nm excitation can measure all ROS (27). Therefore, to investigate the role of MnTE-2-PyP, specifically on superoxide, along with other species of reactive oxygen, we excited the cells with 405 nm for superoxide measurement and with 488 nm for all ROS measurement. We found that 2 Gy X-ray irradiation can significantly increase intracellular superoxide production and MnTE-2-PyP can significantly reduce radiation-induced superoxide levels (Fig. 1A). In addition, all ROS levels increased after irradiation. MnTE-2-PyP treatment significantly reduced the percentage of cells producing all ROS (Fig. 1B). These findings

indicate that MnTE-2-PyP acts as an antioxidant and mainly as a superoxide scavenger in mouse prostate fibroblast cells after irradiation.

MnTE-2-PyP, or NOX4 Inhibition, Prevents Radiation-Induced Cell Size

A prominent feature of a fibroblast activated by irradiation is increased cell size (28). Therefore, we measured cell area after irradiating the prostate fibroblast cells isolated from wild-type and NOX4$^{-/-}$ mice. For the wild-type fibroblasts, cell size was measured in the presence or absence of MnTE-2-PyP. While mean cell size was significantly increased in 2 Gy irradiated wild-type cells treated with PBS compared to nonirradiated cells (Fig. 2A and B), mean cell size was unchanged in the 2 Gy irradiated NOX4$^{-/-}$ fibroblasts and MnTE-2-PyP-treated wild-type fibroblasts (Fig. 2A and B). Thus, according to our findings, NOX4$^{-/-}$ fibroblasts and MnTE-2-PyP-treated fibroblasts were resistant to radiation-induced increased cell size.

MnTE-2-PyP or NOX4 Inhibition, Prevents Radiation- and TGF-β1-Induced Fibroblast Activation

The collagen disc contraction assay is a standard method to measure fibroblast activation (29). An activated fibroblast contracts the collagen disc at an increased rate, while a nonactivated fibroblast does not enhance contraction. TGF-β1 is a potent inducer of fibroblast activation and is, therefore, used as a positive control for the collagen contraction assay. Our study revealed that fibroblasts isolated from wild-type mice are activated by 2 Gy X-ray irradiation or TGF-β1 (5 ng/ml), which results in significant contraction of the collagen discs. On the other hand, both the fibroblasts isolated from NOX4$^{-/-}$ mice and MnTE-2-PyP-treated fibroblasts isolated from wild-type mice prevent radiation and TGF-β1-induced contraction of collagen (Fig. 3A and B). Thus, radiation and TGF-β1-induced activation of fibroblasts can be prevented by either knocking down NOX4 or with MnTE-2-PyP treatment.

Because MnTE-2-PyP inhibited both radiation- and TGF-β1-mediated activation of fibroblasts, we wanted to compare MnTE-2-PyP to a known TGF-β inhibitor. We found that MnTE-2-PyP or SB431542 (a TGF-β1 signaling inhibitor) can protect fibroblast cells equally well from radiation-induced contraction of collagen (Fig. 4A and B). Thus, MnTE-2-PyP has a similar inhibitory effect on TGF-β1 signaling and can protect the fibroblast cells from activation, to the same degree as a specific TGF-β1 signaling inhibitor.

MnTE-2-PyP, or NOX4 Inhibition, Protects from Radiation-Induced Senescence

The SA-β-Gal staining experiment revealed that while 2 Gy X-ray irradiation significantly increased the number of senescent cells in prostate fibroblasts isolated from wild-type C57BL/6 mice, it did not induce senescence in the MnTE-2-PyP-treated fibroblasts nor in fibroblasts isolated from NOX4$^{-/-}$ mice (Fig. 5). Thus, both MnTE-2-PyP treatment and NOX4 inhibition prevented radiation-induced senescence in the mouse primary prostate fibroblast.

Downregulation of Radiation-Induced Profibrotic Gene Expression by MnTE-2-PyP

In this study, radiation-induced activation and senescence of fibroblasts were found to be significantly mitigated by MnTE-2-PyP. Therefore, we investigated the effects of MnTE-2-PyP on the expression of genes involved in profibrotic pathways. We examined the mRNA expression profile of profibrotic genes embedded on Fibrosis Tier 1 M96 PrimePCR array plates (Bio-Rad). To maintain the strict standards of this data analysis, both GAPDH and RPLP0 were used as internal controls for evaluating the relative amplification plot of the test genes. To determine the difference between expression of profibrotic genes after irradiation in the presence and absence of MnTE-2-PyP, a $\log_2$ ratio ≥1.5 was set as the cutoff. After irradiation, it was found that 30 profibrotic genes were downregulated and four genes were upregulated in MnTE-2-PyP-treated cells compared to that of PBS-treated control cells (Fig. 6). Many of these downregulated genes are controlled by the TGF-β signaling pathway.

Extracellular TGF-β1 Measurement

Given that TGF-β1 is such a strong stimulus for radiation-induced fibrosis, we wanted to determine if the levels of secreted TGF-β1 were altered with MnTE-2-PyP treatment or NOX4 inhibition. According to the manufacturer's protocol, all of the extracellular latent TGF-β1 was activated through acidification before the assay was started. Therefore, the result of the assay corresponds to the total level of activated TGF-β1 secreted by the cells. Our assay revealed that 2 Gy irradiation did not alter the extracellular TGF-β1 levels in mouse prostate fibroblast cells compared to nonirradiated cells. Interestingly, the $NOX4^{-/-}$ cells, either sham or 2 Gy irradiated, showed a highly significant decrease (~70%) in extracellular TGF-β1 levels compared to either sham or 2 Gy irradiated wild-type cells. Whereas, with irradiation, MnTE-2-PyP treatment resulted in an insignificant change in extracellular TGF-β1 compared to control. However, in the absence of radiation, MnTE-2-PyP significantly decreased the level of extracellular TGF-β1 compared to control cells (Fig. 7), although the overall reduction was only 35%.

MnTE-2-PyP Suppresses Radiation-Induced TGFβ Receptor Signaling

Since TGF-β receptor signaling is an important mechanism to initiate the fibrotic response after radiation-induced stress, we checked the expression of TGF-β-Smad signaling proteins by Western blot. Although the extracellular TGF-β1 signal was not changed by MnTE-2-PyP, the receptor for TGF-β signaling, Tgfβr2, was reduced by the drug treatment in the presence or absence of radiation (Fig. 8A). Levels of Smad3 (Fig. 8B), phosphorylation of Smad2 (Fig. 8C) along with the total expression level of Smad2 (Fig. 8C) and Smad4 (Fig. 8D), were found to be significantly downregulated by MnTE-2-PyP treatment with 2 Gy irradiation. Since Pai-1 gene expression is regulated by the TGF-β-SMAD signaling system, we checked the expression of Pai-1 to elucidate the status of downstream pathways of the TGF-β1-Smad system. As a consequence of downregulation of TGF-β1-Smad signaling, the expression of TGF-β1 target gene Pai-1 was significantly downregulated by MnTE-2-PyP treatment (Fig. 8F). Smad7 is a TGF-β1 inhibitory molecule and the protein levels of Smad7 were not significantly changed by MnTE-2-PyP treatment (Fig. 8E). We were unable to detect any bands in the immunoblot for phosphorylated Smad3. Therefore, we were unable

to conclude whether MnTE-2-PyP alters the phosphorylation status of Smad3 in our experimental conditions.

NOX4 Inhibition Also Suppresses TGF-β Signaling

Although TGF-β1 levels were significantly reduced, Tgf-βr2 was significantly upregulated in NOX4$^{-/-}$ mouse prostate fibroblasts after 2 Gy irradiation compared to the same without irradiation (Fig. 8A). Phosphorylated Smad2 and total Smad3 were found to be significantly downregulated in NOX4$^{-/-}$ mouse prostate fibroblasts compared to wild-type mouse prostate fibroblasts either with or without irradiation (Fig. 8B and C). The TFG-β1-Smad4 target gene Pai-1 was also significantly downregulated in NOX4$^{-/-}$ mouse prostate fibroblasts compared to wild-type mouse fibroblasts with or without 2 Gy irradiation (Fig. 8F).

Discussion

Proper balance of superoxide production and its dismutation are necessary for maintaining the health of normal tissue after radiation exposure. Superoxide dismutases (SODs) are the primary enzymes for eliminating the effects of superoxide and protect against fibrosis (30). Liposome-mediated delivery of Cu/Zn SOD successfully prevented radiation-induced fibrosis in a published clinical trial (31). However, this therapy relies on the purification of recombinant protein, which is costly and time consuming. MnTE-2-PyP is a low-molecular-weight drug that is relatively inexpensive and easy to produce, and is a SOD mimetic that reduces superoxide levels and has previously been described as a radioprotector in different tissue types (9, 32). MnTE-2-PyP acts as an antioxidant in asthma mouse models and other nonmalignant tissues (33, 34). But in certain malignant cell types, it has been described as pro-oxidant (35, 36). Therefore, to check the mode of action of MnTE-2-PyP in irradiated prostate fibroblast cells, it was necessary to scrutinize its effect on the cellular redox environment. Our data suggest that MnTE-2-PyP scavenges ROS, specifically superoxide, and acts as an antioxidant in fibroblast cells after irradiation.

In our previously published study, we reported that MnTnBuOE-2-PyP, a sister compound of MnTE-2-PyP, can protect colorectal fibroblasts from 2 Gy radiation-induced damage (11). For the current study, we investigated the underlying mechanism of MnTE-2-PyP in protecting normal tissue from radiation-induced fibrosis and senescence. As NOX4 has also been reported as one of the central regulatory molecules for TGF-β-mediated radiation-induced damage and is induced to produce superoxide (37), we used the NOX4$^{-/-}$ mice to examine whether MnTE-2-PyP would protect the normal tissue from radiation in a similar mechanism.

TGF-β1 induces profibrotic gene expression through the activation of SMAD proteins. SMAD proteins act as transcription regulators of profibrotic genes and execute the TGF-β1-mediated fibrosis in cells (38). MAP kinase (Ras/MAP kinase kinase/ERK) signaling cascades have also been reported to activate SMAD signaling after TGF-β1 stimulation (39–42). TGF signaling also includes p38-mitogen-activated protein kinase-mediated signaling in a SMAD-independent manner (43, 44). A single high-dose (15 Gy) of radiation increases the expression of PTEN and reduction of PI3K/AKT signaling in mouse lung tissue. Another

manganese porphyrin molecule, AEOL10150, can reduce radiation-induced PTEN expression (45).

Another important regulator of TGF-β1 signaling is a member of NADPH oxidase family, NOX4. In ROS-mediated fibrotic disease, NOX4 has been studied extensively (46). It has been reported that a positive feedback loop exists between NOX4 and TGF-β1, which produces ROS to convert cardiac fibroblasts into myofibroblasts (47). NOX4 can be activated by PDGF, angiotensin II, TGF-β and TNF-α. Activated NOX4 generates superoxide by carrying electrons from cytosolic NADPH to the membrane, which leads to changes in protein tyrosine kinases, serine/ threonine kinases, phospholipases and calcium-dependent pathways. This ultimately leads to tissue fibrosis (48). It is also reported that NOX4 produces superoxide in the nucleus and executes a direct gene expression regulation via oxidative stress response (49). Radiation-induced cellular senescence has also been reported to be closely regulated by the TGF-NOX4 loop via γ-H2AX-mediated DNA damage response. After irradiation, TGF-β signaling can also result in an increased cell size and fibroblast activation (50, 51).

The TGF-β-Smad signaling axis is the central regulatory pathway that controls radiation-induced fibrosis. TGF-β generally remains dormant through association with the latency associated protein (LAP) in the extracellular region. Exposure to radiation causes dissociation of LAP from TGF-β, which results in TGF-β activation. Activated TGF-β1 then binds to the extracellular region of the TGF-β receptor 2 (TGF-βR2). Ligand-bound TGF-βR2 then heterodimerizes with TGF-βRI, resulting in phosphorylation of receptor-regulated R-SMADs (SMAD2 and SMAD3). Phosphorylated R-SMADs then bind to common-mediator SMAD or co-SMAD, which is SMAD4. These SMAD2-SMAD4 or SMAD3-SMAD4 complexes then translocate to the nucleus and regulate the expression of different target genes of TGF-β by binding to the promoter region of those genes (20). Many of those SMAD-regulated TGF-β target genes (e.g., COL1A1, COL1A2, PAI-1) are the crucial regulators of radiation-induced fibrosis and senescence (Fig. 9) (52–54). One of the major inhibitory molecules of this system is SMAD7, which is also under regulation of the TGF-β-SMAD system, and acts as a self-regulatory molecule for this system.

The extracellular active TGF-β1 level was reported to be higher after irradiation with a single high-dose or recurring lower-dose of radiations. Treatment consisting of a priming dose of 0.1 or 0.5 Gy radiation followed by a challenging dose of 2 Gy 24 h later can significantly upregulate TGF-β1 levels in human primary skin fibroblasts (55). However, there are multiple reports showing that single low dose of radiation failed to significantly increase the extracellular TGF-β1 level. According to a previously published study, in mouse peritoneal macrophages, single low-dose of X-ray radiation (0.01–2 Gy) could not significantly change the extracellular TGF-β1 levels (56). It has also been reported that 2.4 Gy irradiation failed to increase the extracellular TGF-β1 level in human normal skin fibroblast (57). Similarly, our data show that a single dose of 2 Gy radiation does not produce a higher level of TGF-β compared to the control nonirradiated cells. MnTE-2-PyP was previously reported to cause a reduction in elevated plasma TGF-β levels in rats after a single high dose (28 Gy) of radiation to the lung (58). In another published study, another

manganese porphyrin, AEOL10150, was also shown to reduce TGF-β1 and NOX4 levels in 15 Gy irradiated mouse lung tissue (45).

In the current study, MnTE-2-PyP showed significant protection of mouse prostate fibroblast cells after 2 Gy irradiation using the collagen contraction assay, which is considered a standard end measure of fibroblast activation in an *in vitro* model. Our data suggest that MnTE-2-PyP inhibits the TGF-β1 signaling pathway and results in protection from TGF-β1-induced profibrotic and senescent response. MnTE-2-PyP can protect normal fibroblasts from radiation-induced activation to the same degree as a TGF-β receptor 1 inhibitor. TGF-β-targeted therapy is proposed in fibrotic and postirradiation therapy for malignancies (59, 60), but there has been concern that inhibition of TGF-β may be advantageous to the tumor. On the contrary, manganese porphyrins treatment is currently in clinical trials and have demonstrated no significant clinical side effects, and several published *in vivo* tumor studies have indicated that manganese porphyrins do not protect tumor cells from radiation-induced damage (61, 62). Therefore, we can suggest that MnTE-2-PyP can prevent the profibrotic response in irradiated fibroblasts to the same extent as pharmacological TGF-β1 signaling inhibitors without the adverse clinical effect of direct TGF-β1 receptor inhibitors.

These results suggest that MnTE-2-PyP protects mouse prostate fibroblasts from radiation-induced cellular alterations. Profibrotic genes are the executor for initializing fibrosis in irradiated tissue. Therefore, to elucidate the mechanism of radiation-damage protection, our first step was to measure the changes in expression of profibrotic genes after irradiation in the presence of MnTE-2-PyP. mRNA expression of Col1A1, one of the prime indicators of fibrosis, was downregulated by the drug after irradiation. Further, mRNA expression of Tgfβr2 was also downregulated by the drug after irradiation. Since TGF-β is one of the central regulators of profibrotic gene expression, downregulation of Tgfβr2 by MnTE-2-PyP could affect the entire downstream process. Indeed, further studies revealed that MnTE-2-PyP significantly downregulated the protein expression of Tgfβr2, which is the first receptor molecule to initiate TGF-β signaling after irradiation. Although there was a small reduction in extracellular TGF-β levels in the presence of MnTE-2-PyP, there were markedly reduced levels of the receptor molecule, indicating that extracellular TGF-β could not bind to its receptor. As a consequence, there was significant downregulation in the phosphorylation of Smad2. The total expression of Smad2 was also significantly downregulated by MnTE-2-PyP after irradiation; therefore, it is unclear whether downregulation of the phosphorylation of Smad2 is due only to reduced expression of Smad2 protein in the presence of MnTE-2-PyP after irradiation or the phosphorylation event itself was downregulated by the significant downregulation of Tgfβr2. Total protein levels of Smad3 and Smad4 were also found to be downregulated by MnTE-2-PyP treatment. Therefore, this could explain why TGF-β target gene expression is reduced in the presence of MnTE-2-PyP. In agreement with this hypothesis, our results showed that the expression of Pai-1, a TGF-β-inducible gene, was significantly downregulated by MnTE-2-PyP compared to a PBS-treated sample after irradiation. This also explains the observation that, as there are insufficient TGF-β1 receptor molecules present in the MnTE-2-PyP-treated fibroblast cells, the TGF-β1 treatment, which is a potent activator of fibroblasts, also failed to induce fibroblast activation in our collagen contraction assay.

It is possible that after irradiation, inhibition of the TGF-Smad system by MnTE-2-PyP may be triggered by the direct suppression of Tgfβr2 gene expression by MnTE-2-PyP itself at the genomic level or that there is another regulatory molecule involved, which can cause indirect suppression of Tgfβr2 expression after irradiation in MnTE-2-PyP-treated cells.

Surprisingly, the protein expression of inhibitory molecule, Smad7, which is also under control of the TGF-Smad system, was not significantly affected by MnTE-2-PyP. Smad7 is a target molecule of TGF-β1-SMAD signaling and MnTE-2-PyP downregulates the mRNA expression of Smad7 as a result of transcriptional repression of TGF-β1 target genes. Paradoxically, we did not observe a significant decrease in Smad7 protein level. There are previously published studies in which this discrepancy between Smad7 mRNA and protein levels are described. miRNA21, which is an important regulator of fibrosis, can inhibit Smad7 protein translation without altering its mRNA level (63–65). Upregulation of miRNA21 expression has been reported in fibrosis (66, 67). miRNA21 binds to the 3′UTR of Smad7 mRNA and inhibits its translation rather than degrading the mRNA (68). Another important controlling system of the Smad7 protein level in the cell is proper balance between p300 and HDAC1 activity (69). These also alter Smad7 protein stability without affecting the mRNA level. To maintain the negative regulatory effect of Smad7 to TGF-β1-mediated fibrotic response, a minimal level of SMAD7 protein is necessary. Because MnTE-2-PyP can prevent the fibrotic response, it is possible that MnTE-2-PyP could decrease miRNA21 levels, although more experiments are needed to determine if this does occur.

On the other hand, the NOX4$^{-/-}$ prostate fibroblasts were protected against radiation-induced tissue damage by a different mechanism. Unlike MnTE-2-PyP-treated cells, the extracellular TGF-β production was significantly downreg-ulated in NOX4$^{-/-}$ fibroblasts compared to wild-type prostate fibroblasts both before and after irradiation. In addition, the phosphorylation of Smad2 and the expression of total Smad3 proteins were also found to be significantly downregulated in NOX4$^{-/-}$ fibroblasts compared to wild-type mouse prostate fibroblasts. Although there was a significant increase in Tgf-βr2 levels in irradiated NOX4$^{-/-}$ fibroblasts, the expression of the profibrotic gene, Pai-1, was significantly downregulated in both nonirradiated and irradiated NOX4$^{-/-}$ fibroblasts compared to wild-type fibroblasts, presumably due to reduced levels of activated TGF-β1. ROS has been reported to directly dissociate TGF-β from LAP, and therefore increase activated TGF-β levels (70). Induction of NOX4 expression by TGF-β results in ROS production, which in turn further activates and maintains TGF-β signaling (71, 72).

NOX4 and MnTE-2-PyP may have different effects on the TGF-β signaling pathways due to differences in localization. NOX4 is localized to membranes and is likely producing ROS into the extracellular space, so in irradiated wild-type cells, the NOX4 enzyme is likely producing ROS that can cleave the LAP protein, which results in activated TGF-β1. When NOX4 is removed from this system, the extracellular ROS is not produced and TGF-β1 is not activated. In contrast, MnTE-2-PyP is not lipophilic, but is instead present inside cellular compartments such as the nucleus, mitochondria, as well as in the cytoplasm. Therefore, MnTE-2-PyP may not be affecting extracellular ROS levels but may instead be affecting redox signaling inside the cell, which results in the reduction of the Tgfβr2 levels. One

potential mechanism may be altering AP-1 activity, a known redox-sensitive transcription factor, which binds to the promotor of Tgfβr2. However, more experiments are needed to determine if this hypothesis is correct.

In summary, the results of this study suggest that MnTE-2-PyP downregulates TGF-β receptor signaling by inhibiting the expression of TGF-βR2, SMAD2, SMAD3, SMAD4 and phosphorylation of SMAD2. While in $NOX4^{-/-}$ fibroblasts, the expression of extracellular TGF-β1, as well as SMAD3 and phosphorylation of SMAD2, are downregulated. As a consequence, the inhibition of profibrotic gene expression after irradiation protects normal fibroblasts from radiation-induced tissue damage in both of these models (Fig. 9).

The major regulatory pathway for radiation-induced change of morphology, fibrosis and senescence is the TGF-β-SMAD signaling pathway. This study suggests that MnTE-2-PyP significantly downregulates radiation-induced normal tissue damage by inhibiting TGF-β-SMAD signaling through superoxide scavenging. These findings support the use of MnTE-2-PyP as a radioprotector during radiation therapy for prostate cancer.

Acknowledgments

This work was supported by the National Institutes of Health (grant no. 1R01CA178888) and the Fred and Pamela Buffet Cancer Center (grant no. P30CA036727). Dr. Oberley-Deegan is a consultant with BioMimetix Pharmaceutical, Inc. and holds equities in BioMimetix Pharmaceutical, Inc.

References

1. Siegel R, Naishadham D, Jemal A. Cancer statistics, 2012. CA Cancer J Clin. 2012; 62:10–29. [PubMed: 22237781]
2. Elliott SP, Malaeb BS. Long-term urinary adverse effects of pelvic radiotherapy. World J Urol. 2011; 29:35–41. [PubMed: 20959990]
3. Sullivan L, Williams SG, Tai KH, Foroudi F, Cleeve L, Duchesne GM. Urethral stricture following high dose rate brachytherapy for prostate cancer. Radiother Oncol. 2009; 91:232–6. [PubMed: 19097660]
4. Ghisolfi L, Keates AC, Hu X, Lee DK, Li CJ. Ionizing radiation induces stemness in cancer cells. PLoS One. 2012; 7:e43628. [PubMed: 22928007]
5. Matsumoto H, Hayashi S, Hatashita M, Ohnishi K, Shioura H, Ohtsubo T, et al. Induction of radioresistance by a nitric oxide-mediated bystander effect. Radiat Res. 2001; 155:387–96. [PubMed: 11182788]
6. Sabin RJ, Anderson RM. Cellular senescence - its role in cancer and the response to ionizing radiation. Genome Integr. 2011; 2:7. [PubMed: 21834983]
7. Weigel C, Schmezer P, Plass C, Popanda O. Epigenetics in radiation-induced fibrosis. Oncogene. 2015; 34:2145–55. [PubMed: 24909163]
8. Yarnold J, Brotons MC. Pathogenetic mechanisms in radiation fibrosis. Radiother Oncol. 2010; 97:149–61. [PubMed: 20888056]
9. Oberley-Deegan RE, Steffan JJ, Rove KO, Pate KM, Weaver MW, Spasojevic I, et al. The antioxidant, MnTE-2-PyP, prevents side-effects incurred by prostate cancer irradiation. PLoS One. 2012; 7:e44178. [PubMed: 22984473]
10. Tong Q, Weaver MR, Kosmacek EA, O'Connor BP, Harmacek L, Venkataraman S, et al. MnTE-2-PyP reduces prostate cancer growth and metastasis by suppressing p300 activity and p300/HIF-1/CREB binding to the promoter region of the PAI-1 gene. Free Radic Biol Med. 2016; 94:185–94. [PubMed: 26944191]

11. Kosmacek EA, Chatterjee A, Tong Q, Lin C, Oberley-Deegan RE. MnTnBuOE-2-PyP protects normal colorectal fibroblasts from radiation damage and simultaneously enhances radio/chemotherapeutic killing of colorectal cancer cells. Oncotarget. 2016; 7:34532–45. [PubMed: 27119354]
12. Barnes JL, Gorin Y. Myofibroblast differentiation during fibrosis: role of NAD(P)H oxidases. Kidney Int. 2011; 79:944–56. [PubMed: 21307839]
13. Bondi CD, Manickam N, Lee DY, Block K, Gorin Y, Abboud HE, et al. NAD(P)H oxidase mediates TGF-beta1-induced activation of kidney myofibroblasts. J Am Soc Nephrol. 2010; 21:93–102. [PubMed: 19926889]
14. Chan EC, Peshavariya HM, Liu GS, Jiang F, Lim SY, Dusting GJ. Nox4 modulates collagen production stimulated by transforming growth factor beta1 in vivo and in vitro. Biochem Biophys Res Commun. 2013; 430:918–25. [PubMed: 23261430]
15. Cucoranu I, Clempus R, Dikalova A, Phelan PJ, Ariyan S, Dikalov S, et al. NAD(P)H oxidase 4 mediates transforming growth factor-beta1-induced differentiation of cardiac fibroblasts into myofibro-blasts. Circ Res. 2005; 97:900–7. [PubMed: 16179589]
16. Hecker L, Vittal R, Jones T, Jagirdar R, Luckhardt TR, Horowitz JC, et al. NADPH oxidase-4 mediates myofibroblast activation and fibrogenic responses to lung injury. Nat Med. 2009; 15:1077–81. [PubMed: 19701206]
17. Samarakoon R, Overstreet JM, Higgins PJ. TGF-beta signaling in tissue fibrosis: redox controls, target genes and therapeutic opportunities. Cell Signal. 2013; 25:264–8. [PubMed: 23063463]
18. Sampson N, Berger P, Zenzmaier C. Therapeutic targeting of redox signaling in myofibroblast differentiation and age-related fibrotic disease. Oxid Med Cell Longev. 2012; 2012:458276. [PubMed: 23150749]
19. Amara N, Goven D, Prost F, Muloway R, Crestani B, Boczkowski J. NOX4/NADPH oxidase expression is increased in pulmonary fibroblasts from patients with idiopathic pulmonary fibrosis and mediates TGFbeta1-induced fibroblast differentiation into myofibroblasts. Thorax. 2010; 65:733–8. [PubMed: 20685750]
20. Dancea HC, Shareef MM, Ahmed MM. Role of radiation-induced TGF-beta signaling in cancer therapy. Mol Cell Pharmacol. 2009; 1:44–56. [PubMed: 20336170]
21. Martin M, Lefaix J, Delanian S. TGF-beta1 and radiation fibrosis: a master switch and a specific therapeutic target? Int J Radiat Oncol Biol Phys. 2000; 47:277–90. [PubMed: 10802350]
22. Andarawewa KL, Paupert J, Pal A, Barcellos-Hoff MH. New rationales for using TGFbeta inhibitors in radiotherapy. Int J Radiat Biol. 2007; 83:803–11. [PubMed: 18058368]
23. Anscher MS. Targeting the TGF-beta1 pathway to prevent normal tissue injury after cancer therapy. Oncologist. 2010; 15:350–9. [PubMed: 20413640]
24. Seluanov A, Vaidya A, Gorbunova V. Establishing primary adult fibroblast cultures from rodents. J Vis Exp. 2010
25. Schneider CA, Rasband WS, Eliceiri KW. NIH Image to ImageJ: 25 years of image analysis. Nat Methods. 2012; 9:671–5. [PubMed: 22930834]
26. Eccles M, Li CG. Senescence associated beta-galactosidase staining. Bio-Protocol. 2012; 2:e247.
27. Nazarewicz RR, Bikineyeva A, Dikalov SI. Rapid and specific measurements of superoxide using fluorescence spectroscopy. J Biomol Screen. 2013; 18:498–503. [PubMed: 23190737]
28. Vergara JA, Raymond U, Thet LA. Changes in lung morphology and cell number in radiation pneumonitis and fibrosis: a quantitative ultrastructural study. Int J Radiat Oncol Biol Phys. 1987; 13:723–32. [PubMed: 3570895]
29. Montesano R, Orci L. Transforming growth factor beta stimulates collagen-matrix contraction by fibroblasts: implications for wound healing. Proc Natl Acad Sci U S A. 1988; 85:4894–7. [PubMed: 3164478]
30. Gao F, Kinnula VL, Myllarniemi M, Oury TD. Extracellular superoxide dismutase in pulmonary fibrosis. Antioxid Redox Signal. 2008; 10:343–54. [PubMed: 17999630]
31. Delanian S, Baillet F, Huart J, Lefaix JL, Maulard C, Housset M. Successful treatment of radiation-induced fibrosis using liposomal Cu/Zn superoxide dismutase: clinical trial. Radiother Oncol. 1994; 32:12–20. [PubMed: 7938674]

32. Archambeau JO, Tovmasyan A, Pearlstein RD, Crapo JD, Batinic-Haberle I. Superoxide dismutase mimic, MnTE-2-PyP(5+) ameliorates acute and chronic proctitis following focal proton irradiation of the rat rectum. Redox Biol. 2013; 1:599–607. [PubMed: 24363995]
33. Jungsuwadee P, Weaver MR, Gally F, Oberley-Deegan RE. The metalloporphyrin antioxidant, MnTE-2-PyP, inhibits Th2 cell immune responses in an asthma model. Int J Mol Sci. 2012; 13:9785–97. [PubMed: 22949830]
34. Terziev L, Dancheva V, Shopova V, Stavreva G. Antioxidant effect of MnTE-2-PyP on lung in asthma mice model. ScientificWorldJournal. 2012; 2012:379360. [PubMed: 22654599]
35. Jaramillo MC, Briehl MM, Crapo JD, Batinic-Haberle I, Tome ME. Manganese porphyrin, MnTE-2-PyP5+, Acts as a pro-oxidant to potentiate glucocorticoid-induced apoptosis in lymphoma cells. Free Radic Biol Med. 2012; 52:1272–84. [PubMed: 22330065]
36. Tong Q, Zhu Y, Galaske JW, Kosmacek EA, Chatterjee A, Dickinson BC, et al. MnTE-2-PyP modulates thiol oxidation in a hydrogen peroxide-mediated manner in a human prostate cancer cell. Free Radic Biol Med. 2016; 101:32–43. [PubMed: 27671770]
37. Hubackova S, Krejcikova K, Bartek J, Hodny Z. IL1- and TGFbeta-Nox4 signaling, oxidative stress and DNA damage response are shared features of replicative, oncogene-induced, and drug-induced paracrine 'bystander senescence'. Aging (Albany NY). 2012; 4:932–51. [PubMed: 23385065]
38. Bentzen SM. Preventing or reducing late side effects of radiation therapy: radiobiology meets molecular pathology. Nat Rev Cancer. 2006; 6:702–13. [PubMed: 16929324]
39. Kamaraju AK, Roberts AB. Role of Rho/ROCK and p38 MAP kinase pathways in transforming growth factor-beta-mediated Smad-dependent growth inhibition of human breast carcinoma cells in vivo. J Biol Chem. 2005; 280:1024–36. [PubMed: 15520018]
40. Matsuura I, Wang G, He D, Liu F. Identification and characterization of ERK MAP kinase phosphorylation sites in Smad3. Biochemistry. 2005; 44:12546–53. [PubMed: 16156666]
41. Ross KR, Corey DA, Dunn JM, Kelley TJ. SMAD3 expression is regulated by mitogen-activated protein kinase kinase-1 in epithelial and smooth muscle cells. Cell Signal. 2007; 19:923–31. [PubMed: 17197157]
42. Ventura JJ, Kennedy NJ, Flavell RA, Davis RJ. JNK regulates autocrine expression of TGF-beta1. Mol Cell. 2004; 15:269–78. [PubMed: 15260977]
43. Chen RH, Chang MC, Su YH, Tsai YT, Kuo ML. Interleukin-6 inhibits transforming growth factor-beta-induced apoptosis through the phosphatidylinositol 3-kinase/Akt and signal transducers and activators of transcription 3 pathways. J Biol Chem. 1999; 274:23013–9. [PubMed: 10438468]
44. Chen RH, Su YH, Chuang RL, Chang TY. Suppression of transforming growth factor-beta-induced apoptosis through a phosphatidylinositol 3-kinase/Akt-dependent pathway. Oncogene. 1998; 17:1959–68. [PubMed: 9788439]
45. Zhang Y, Zhang X, Rabbani ZN, Jackson IL, Vujaskovic Z. Oxidative stress mediates radiation lung injury by inducing apoptosis. Int J Radiat Oncol Biol Phys. 2012; 83:740–8. [PubMed: 22270165]
46. Jiang F, Liu GS, Dusting GJ, Chan EC. NADPH oxidase-dependent redox signaling in TGF-beta-mediated fibrotic responses. Redox Biol. 2014; 2:267–72. [PubMed: 24494202]
47. MacLean J, Pasumarthi KB. Signaling mechanisms regulating fibroblast activation, phenoconversion and fibrosis in the heart. Indian J Biochem Biophys. 2014; 51:476–82. [PubMed: 25823219]
48. Gorin Y, Ricono JM, Kim NH, Bhandari B, Choudhury GG, Abboud HE. Nox4 mediates angiotensin II-induced activation of Akt/protein kinase B in mesangial cells. Am J Physiol Renal Physiol. 2003; 285:F219–29. [PubMed: 12842860]
49. Kuroda J, Nakagawa K, Yamasaki T, Nakamura K, Takeya R, Kuribayashi F, et al. The superoxide-producing NAD(P)H oxidase Nox4 in the nucleus of human vascular endothelial cells. Genes Cells. 2005; 10:1139–51. [PubMed: 16324151]
50. Lamouille S, Derynck R. Cell size and invasion in TGF-beta-induced epithelial to mesenchymal transition is regulated by activation of the mTOR pathway. J Cell Biol. 2007; 178:437–51. [PubMed: 17646396]

51. Skog S, Tribukait B. Cell size following irradiation in relation to cell cycle. Acta Radiol Oncol. 1986; 25:269–73. [PubMed: 3030055]
52. Chen CZ, Raghunath M. Focus on collagen: in vitro systems to study fibrogenesis and antifibrosis state of the art. Fibrogenesis Tissue Repair. 2009; 2:7. [PubMed: 20003476]
53. Ghosh AK, Vaughan DE. PAI-1 in tissue fibrosis. J Cell Physiol. 2012; 227:493–507. [PubMed: 21465481]
54. Raghu G, Masta S, Meyers D, Narayanan AS. Collagen synthesis by normal and fibrotic human lung fibroblasts and the effect of transforming growth factor-beta. Am Rev Respir Dis. 1989; 140:95–100. [PubMed: 2751176]
55. Dieriks B, De Vos W, Baatout S, Van Oostveldt P. Repeated exposure of human fibroblasts to ionizing radiation reveals an adaptive response that is not mediated by interleukin-6 or TGF-beta. Mutat Res. 2011; 715:19–24. [PubMed: 21784085]
56. Wunderlich R, Ernst A, Rodel F, Fietkau R, Ott O, Lauber K, et al. Low and moderate doses of ionizing radiation up to 2 Gy modulate transmigration and chemotaxis of activated macrophages, provoke an anti-inflammatory cytokine milieu, but do not impact upon viability and phagocytic function. Clin Exp Immunol. 2015; 179:50–61. [PubMed: 24730395]
57. Akudugu JM, Bell RS, Catton C, Davis AM, Griffin AM, O'Sullivan B, et al. Wound healing morbidity in STS patients treated with preoperative radiotherapy in relation to in vitro skin fibroblast radiosensitivity, proliferative capacity and TGF-beta activity. Radiother Oncol. 2006; 78:17–26. [PubMed: 16380182]
58. Vujaskovic Z, Batinic-Haberle I, Rabbani ZN, Feng QF, Kang SK, Spasojevic I, et al. A small molecular weight catalytic metallo-porphyrin antioxidant with superoxide dismutase (SOD) mimetic properties protects lungs from radiation-induced injury. Free Radic Biol Med. 2002; 33:857–63. [PubMed: 12208373]
59. Connolly EC, Freimuth J, Akhurst RJ. Complexities of TGF-beta targeted cancer therapy. Int J Biol Sci. 2012; 8:964–78. [PubMed: 22811618]
60. Varga J, Pasche B. Antitransforming growth factor-beta therapy in fibrosis: recent progress and implications for systemic sclerosis. Curr Opin Rheumatol. 2008; 20:720–8. [PubMed: 18946334]
61. Ashcraft KA, Boss MK, Tovmasyan A, Roy Choudhury K, Fontanella AN, Young KH, et al. Novel manganese-porphyrin superoxide dismutase-mimetic widens the therapeutic margin in a preclinical head and neck cancer model. Int J Radiat Oncol Biol Phys. 2015; 93:892–900. [PubMed: 26530759]
62. Gad SC, Sullivan DW Jr, Crapo JD, Spainhour CB. A nonclinical safety assessment of MnTE-2-PyP, a manganese porphyrin. Int J Toxicol. 2013; 32:274–87. [PubMed: 23704100]
63. Loboda A, Sobczak M, Jozkowicz A, Dulak J. TGF-beta1/Smads and miR-21 in renal fibrosis and inflammation. Mediators Inflamm. 2016; 2016:8319283. [PubMed: 27610006]
64. Zhong X, Chung AC, Chen HY, Meng XM, Lan HY. Smad3-mediated upregulation of miR-21 promotes renal fibrosis. J Am Soc Nephrol. 2011; 22:1668–81. [PubMed: 21852586]
65. Zhu H, Luo H, Li Y, Zhou Y, Jiang Y, Chai J, et al. MicroRNA-21 in scleroderma fibrosis and its function in TGF-beta-regulated fibrosis-related genes expression. J Clin Immunol. 2013; 33:1100–9. [PubMed: 23657402]
66. Kwon OS, Kim KT, Lee E, Kim M, Choi SH, Li H, et al. Induction of MiR-21 by stereotactic body radiotherapy contributes to the pulmonary fibrotic response. PLoS One. 2016; 11:e0154942. [PubMed: 27171163]
67. Li S, Liu W, Lei Y, Long J. Regulatory effects of electronic beam irradiation on mir-21/smad7-mediated collagen I synthesis in keloid-derived fibroblasts. Biol Open. 2016; 5:1567–74. [PubMed: 27694104]
68. Li Q, Zhang D, Wang Y, Sun P, Hou X, Larner J, et al. MiR-21/ Smad 7 signaling determines TGF-beta1-induced CAF formation. Sci Rep. 2013; 3:2038. [PubMed: 23784029]
69. Simonsson M, Heldin CH, Ericsson J, Gronroos E. The balance between acetylation and deacetylation controls Smad7 stability. J Biol Chem. 2005; 280:21797–803. [PubMed: 15831498]
70. Krstic J, Trivanovic D, Mojsilovic S, Santibanez JF. Transforming growth factor-beta and oxidative stress interplay: implications in tumorigenesis and cancer progression. Oxid Med Cell Longev. 2015; 2015:654594. [PubMed: 26078812]

71. Hu T, Ramachandrarao SP, Siva S, Valancius C, Zhu Y, Mahadev K, et al. Reactive oxygen species production via NADPH oxidase mediates TGF-beta-induced cytoskeletal alterations in endothelial cells. Am J Physiol Renal Physiol. 2005; 289:F816–25. [PubMed: 16159901]

72. Liu RM, Desai LP. Reciprocal regulation of TGF-beta and reactive oxygen species: A perverse cycle for fibrosis. Redox Biol. 2015; 6:565–77. [PubMed: 26496488]

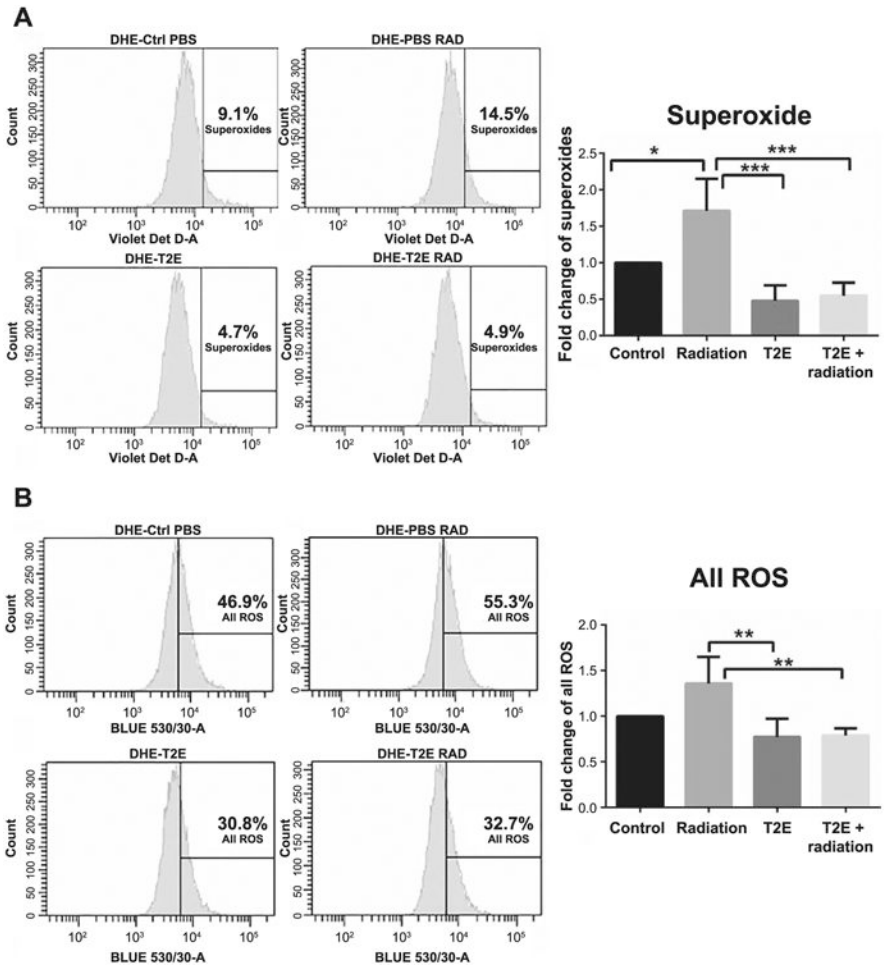

Fig. 1.

MnTE-2-PyP reduces the levels of ROS, including superoxide, after irradiation. Two-week-old primary prostate fibroblast cells were either sham irradiated or 2 Gy X-ray irradiated in the presence or absence of 30 μ*M* MnTE-2-PyP or an equal volume of PBS. Cells were stained with DHE and subjected to flow cytometric analysis. Panel A: Superoxide measurement (405 nm). The percentage of cells producing superoxide was significantly higher in irradiated cells compared to control ($P = 0.0101$) and superoxide production was significantly lower in MnTE-2-PyP-treated irradiated cells ($P = 0.0002$) compared to PBS-treated irradiated cells. Panel B: All ROS measurements (488 nm). The percentage of cells producing all ROS is significantly lower in MnTE-2-PyP-treated irradiated cells ($P = 0.0044$) compared to PBS-treated irradiated cells. The data are representative of three independent experiments and are presented as the mean ± the standard deviation. Significance was determined using one-way ANOVA followed by post hoc Tukey's test for multiple comparisons.

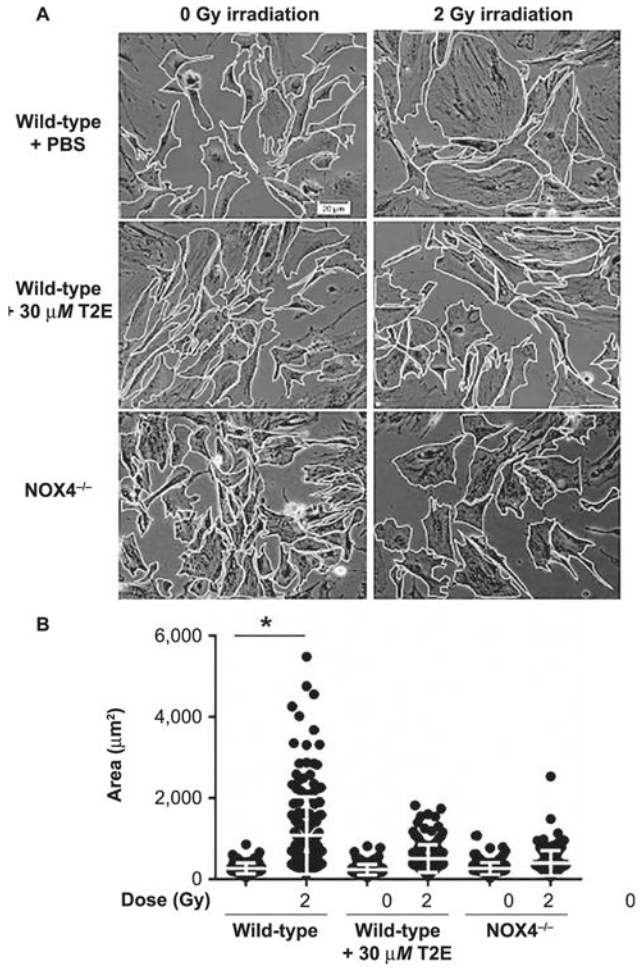

Fig. 2.

MnTE-2-PyP and NOX4$^{-/-}$ inhibits radiation-induced increase in cell size of primary prostate fibroblasts. Panel A: Images of mouse prostate fibroblasts maintained in media with PBS or 30 μ*M* MnTE-2-PyP (for wild-type mouse prostate fibroblasts) were either sham or 2 Gy X-ray irradiated. After 48 h, cells were imaged and their borders were manually traced in ImageJ to calculate cell areas. Panel B: The mean cell area was increased significantly ($P < 0.0001$) in 2 Gy irradiated wild-type cells compared to nonirradiated cells. Irradiated cells treated with MnTE-2-PyP or NOX4$^{-/-}$ were significantly smaller in size compared to wild-type irradiated cells. The combined data of three independent experiments are presented as the mean ± standard deviation. Significance was determined using one-way ANOVA followed by post hoc Tukey's test for multiple comparisons.

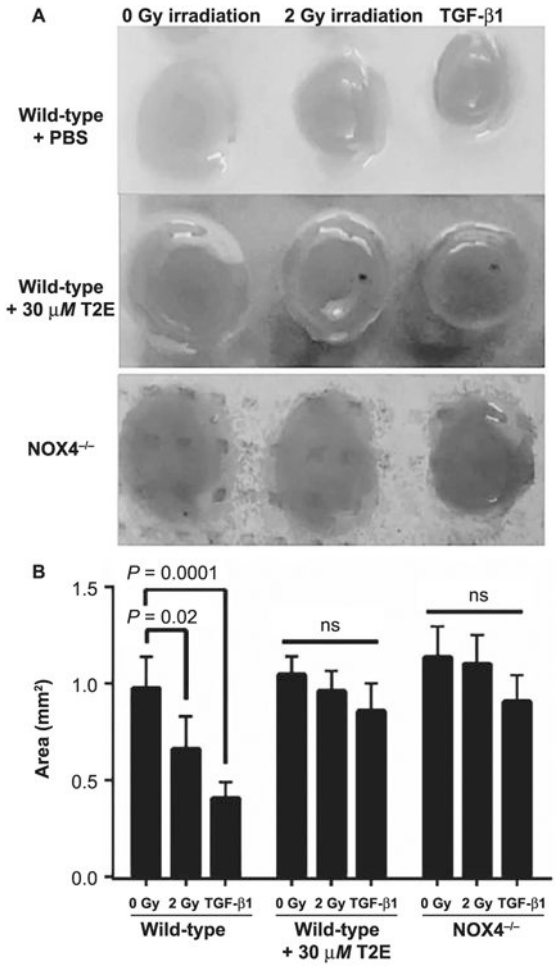

Fig. 3.

MnTnTE-2-PyP and NOX4$^{-/-}$ prevents contraction of collagen by primary prostate fibroblasts. Panel A: Mouse primary prostate fibroblasts were grown in rat collagen discs. Wild-type fibroblasts grown in either PBS or 30 μ*M* MnTE-2-PyP were either 2 Gy X-ray irradiated or treated with 5 ng/ml TGF-β1. NOX4$^{-/-}$ fibroblasts were either 2 Gy X-ray irradiated or treated with 5 ng/ml TGF-β1. Panel B: Collagen disc area measurements were performed with ImageJ. Collagen discs were significantly contracted in wild-type 2 Gy irradiated fibroblasts (*P*=0.02) and TGF-β1 (*P*=0.0001). There was no significant change in collagen disc contraction in cells treated with MnTE-2-PyP or cells lacking NOX4. All data are representative of the mean and standard deviation and were obtained from three independent experiments. *P* values and significance were determined using one-way ANOVA followed by post hoc Tukey's test for multiple comparisons.

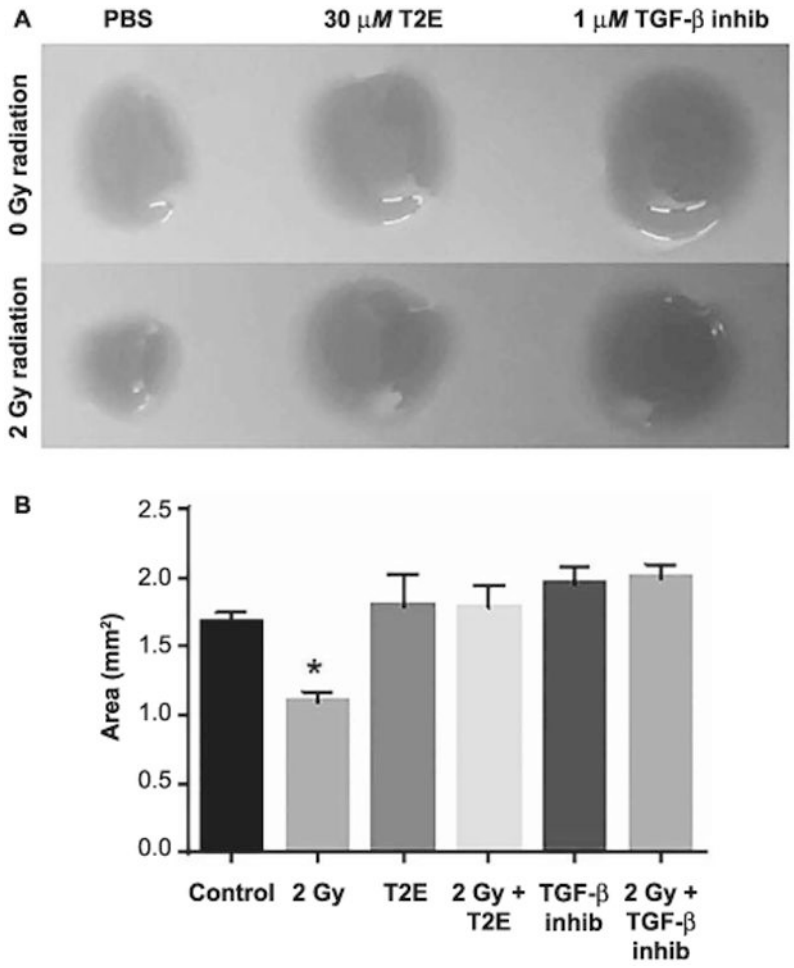

Fig. 4.

MnTE-2-PyP can prevent contraction of collagen to the same degree of direct TGF-β1 inhibition. Panel A: Mouse primary prostate fibroblasts were grown in rat collagen discs. Fibroblasts grown in either 30 μ*M* MnTE-2-PyP or 1 μ*M* SB431542 (TGF-β Inhb.) or equal volume of PBS were either sham or 2 Gy X-ray irradiated. Panel B: Collagen disc area measurements were performed with ImageJ. Collagen discs were significantly contracted after 2 Gy irradiation ($P = 0.0002$). There was no significant change in collagen disc contraction in MnTE-2-PyP- or TGF-β Inhb-treated cells. All data are represented by the mean ± standard deviation and were obtained from three independent experiments. *P* values and significance were determined using one-way ANOVA followed by post hoc Tukey's test for multiple comparisons.

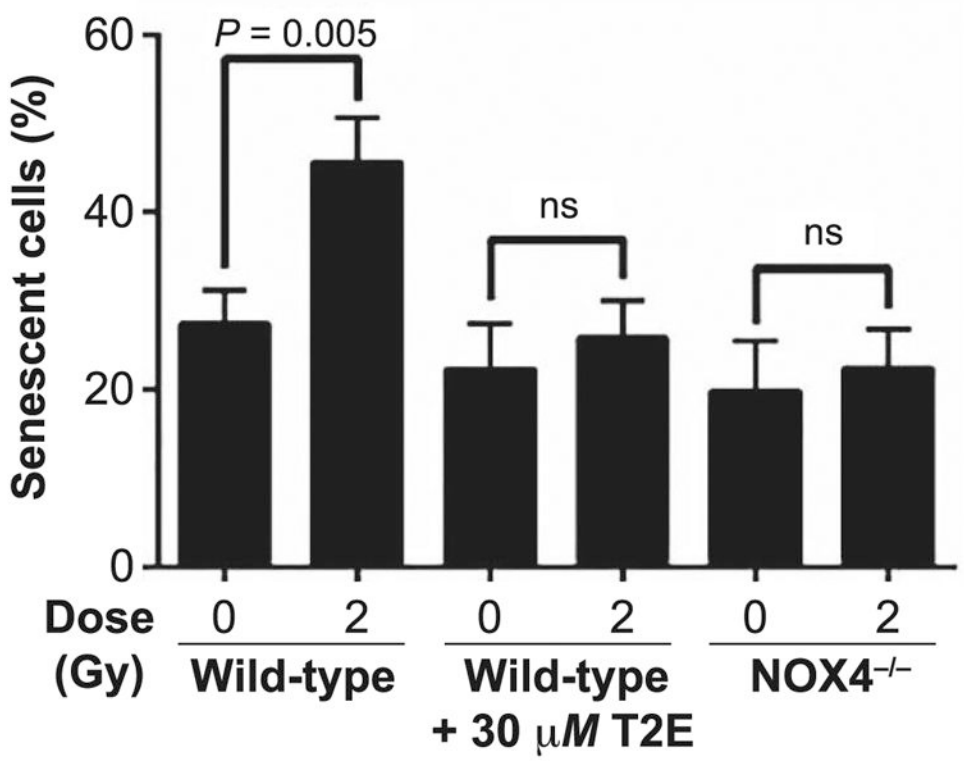

Fig. 5.

MnTnTE-2-PyP and NOX4$^{-/-}$ prevents radiation-induced senescence in primary prostate fibroblasts. Mouse prostate fibroblasts maintained in media with PBS or 30 μ*M* MnTE-2-PyP (for wild-type mice prostate fibroblasts) were either sham or 2 Gy X-ray irradiated, and 48 h later, cells were stained for SA-β-gal expression. Cells were imaged with an inverted brightfield microscope. SA-β-gal expression was significantly increased ($P = 0.005$) in 2 Gy irradiated control cells compared to the nonirradiated population. In wild-type cells, grown in MnTE-2-PyP, and the NOX4$^{-/-}$ cells showed no significant increase in SA-β-gal expression after irradiation. All data are represented by the mean ± standard deviation and were obtained from three independent experiments. The differences of the percentage mean of senescent cells were analyzed for significance using one-way ANOVA followed by post hoc Tukey's test for multiple comparisons.

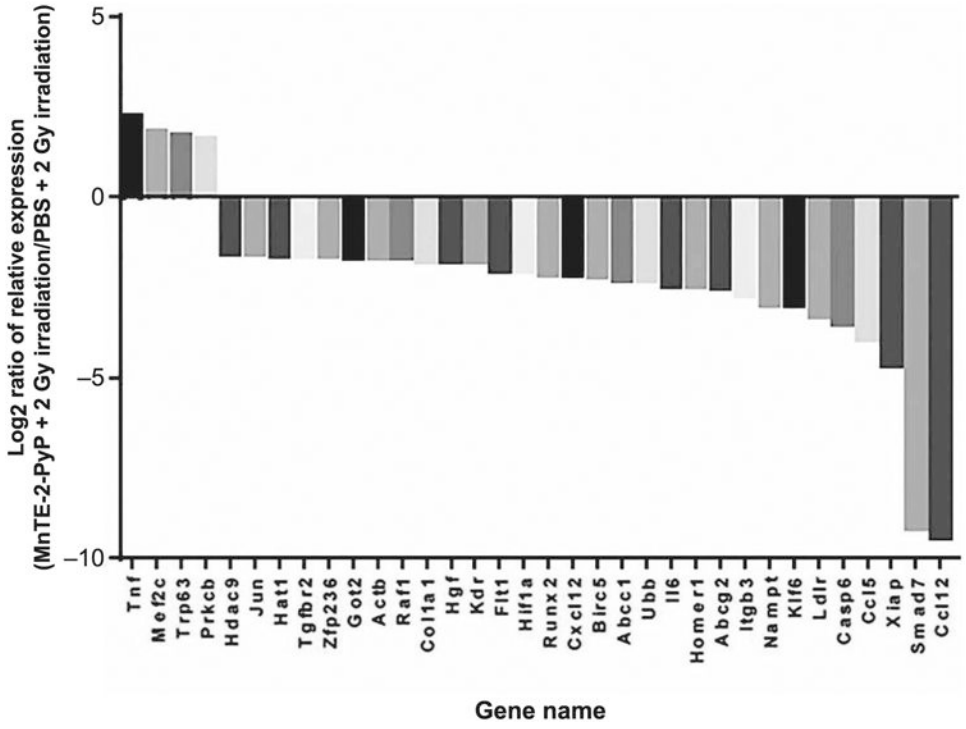

Fig. 6.

Expression profile of a panel of profibrotic genes. Mouse prostate fibroblasts maintained in media with PBS or 30 μ*M* MnTE-2-PyP were 2 Gy X-ray irradiated. Log_2 data (normalized with GAPDH and RPLPO) of mRNA expression profile of profibrotic genes in the Fibrosis Tier 1 M96 PrimePCR array plates in the MnTE-2-PyP-treated irradiated samples were plotted against the PBS-treated irradiated sample. Log_2 ratio ≥1.5 was set as the cutoff.

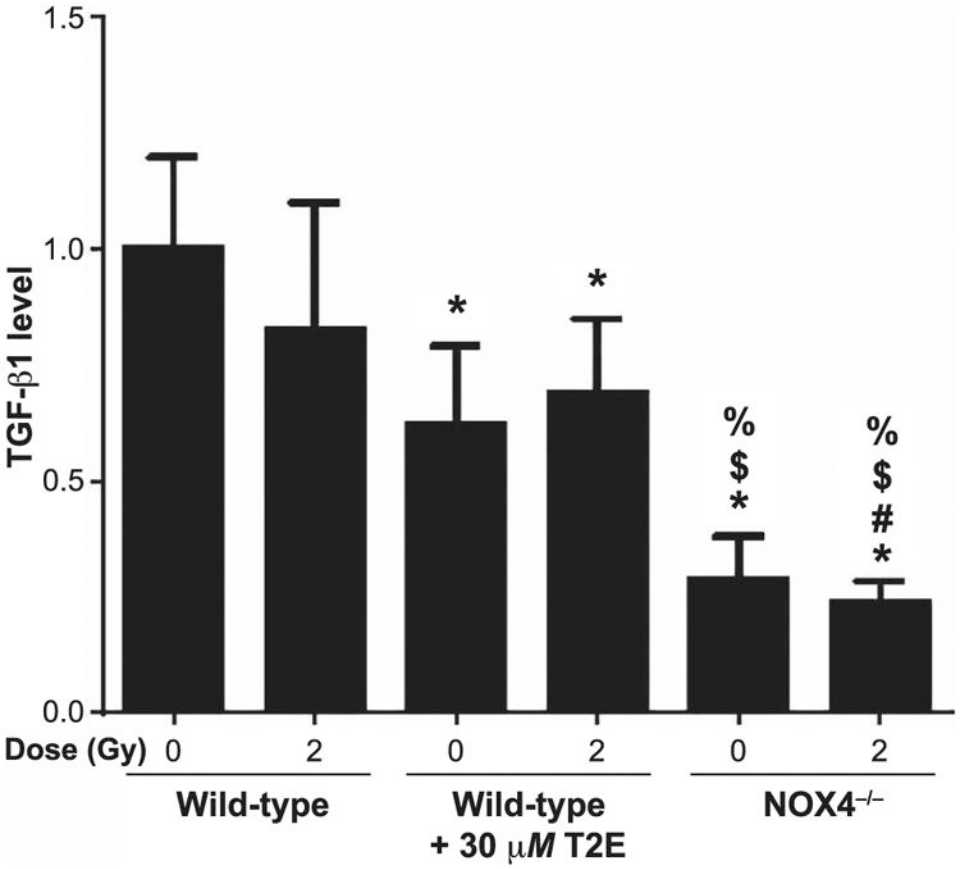

Fig. 7.

Measurement of extracellular TGF-β1. Conditioned media from PBS- or 30 μ*M* MnTE-2-PyP (T2E)-treated wild-type mouse prostate fibroblasts and NOX4$^{-/-}$ mouse prostate fibroblasts were subjected to an activated TGF-β1 ELISA after activation of extracellular TGF-β1 by acidification. The data represent a fold change value of raw absorbance at 450 nm (subtracted by absorbance value at 540 nm). Data represent the mean ± standard deviation and were obtained from three independent experiments. The differences of mean absorbance were analyzed for significance using one-way ANOVA followed by post hoc Holm-Sidak correction for multiple comparisons. *Significant difference compared to wild-type nonirradiated fibroblasts; $^{\#}$significant difference compared to wild-type 2 Gy irradiated fibroblasts; $^{\$}$significant difference compared to T2E-treated nonirradiated fibroblasts; and $^{\%}$significant difference compared to T2E-treated 2 Gy irradiated fibroblasts.

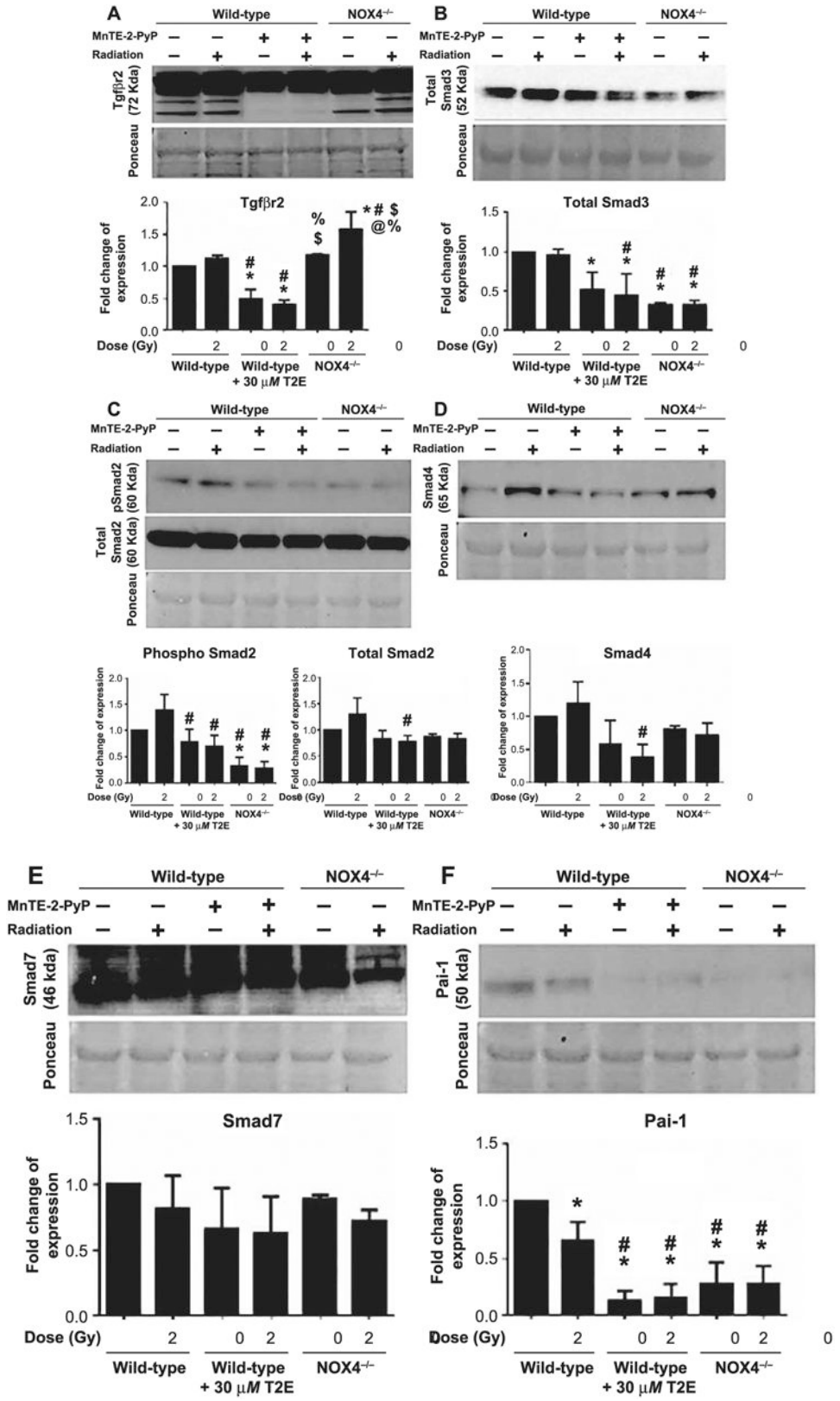

Fig. 8.

TGF-β1 signaling protein expression. Total protein (40 μg) was used for Western blotting. Equal loading of protein was confirmed by Ponceau staining of the blot. All blots were quantified in ImageJ. Fold change over wild-type nonirradiated data was plotted. Figure represents the scanned blot, corresponding Ponceau picture and the quantified data for Tgfβr2 (panel A), total Smad3 (panel B), phospho-Smad2 and total Smad2 (panel C), Smad4 (panel D), Smad7 (panel E) and Pai-1 (panel F). Significance in protein expression levels were calculated using one-way ANOVA followed by post hoc Holm-Sidak correction for multiple comparisons. *Significant difference compared to wild-type nonirradiated fibroblasts; $^{\#}$significant difference compared to wild-type 2 Gy irradiated fibroblasts; $^{\$}$significant difference compared to T2E-treated nonirradiated fibroblasts; $^{\%}$significant difference compared to T2E-treated 2 Gy irradiated fibroblasts; and $^{@}$significant difference compared to NOX4$^{-/-}$ nonirradiated fibroblasts.

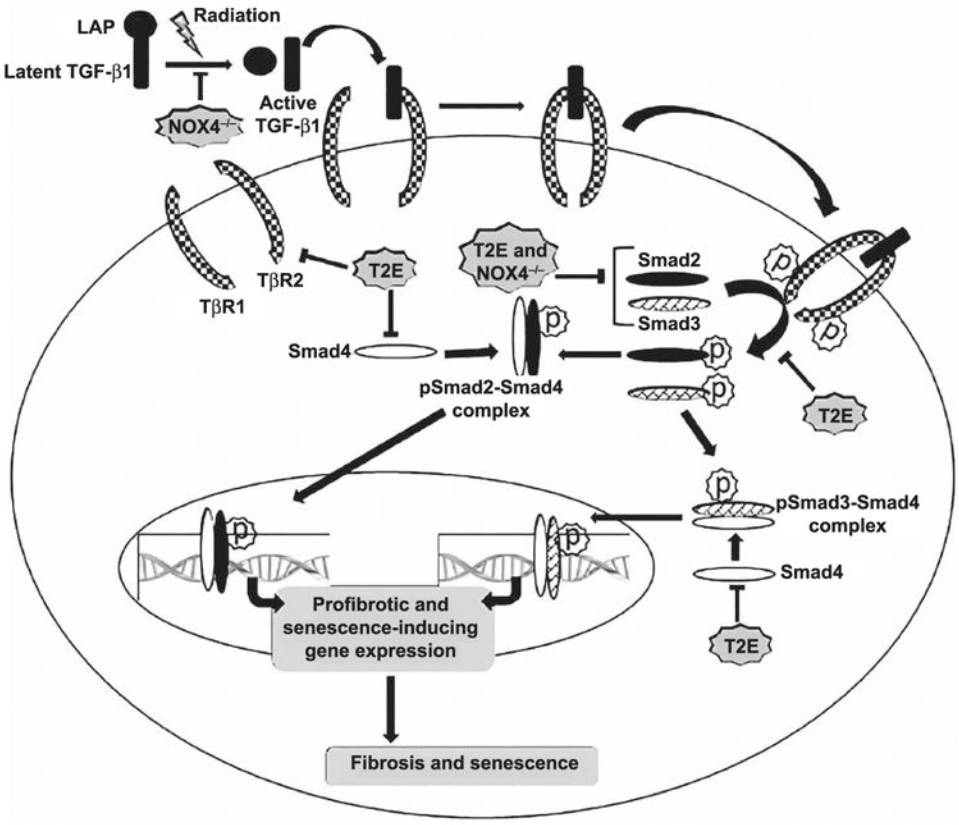

Fig. 9.

Graphical summary of the results. Radiation activates latent TGF-β1 by detaching it from the latency-associated protein (LAP). Activated TGF-β1 binds to TGF-βR2. TGF-βR1 then binds to TGF-βR2. Heterodimerized TGF-β receptors then phosphorylate SMAD2 and SMAD3 in the cytosol. Phosphorylated SMADs then localize to the nucleus after dimerizing with SMAD4. pSMAD2-SMAD4 and pSMAD3-SMAD4 then bind to the promoter region of their target genes and initiate profibrotic and senescence-inducing gene expression. Inhibition of NOX4 inhibits expression of extracellular TGF-b1 and total SMAD3 as well as phosphorylation of SMAD2. MnTE-2-PyP (T2E) inhibits expression of TGF-βR2, SMAD2, SMAD3, SMAD4 and the phosphorylation of SMAD2. As a result, in both of the conditions, inhibition of NOX4 and T2E treatment, profibrotic- and senescence-inducing gene expression is inhibited. As a consequence, inhibition of NOX4 or MnTE-2-PyP-treated irradiated cells become protected from radiation-induced fibrosis and senescence.